Plastic scintillation detectors for precision Time-of-Flight measurements of relativistic heavy ions*

Wen-Jian Lin(林文健)[1] Jian-Wei Zhao(赵建伟)[1] Bao-Hua Sun(孙保华)[1;1)] Liu-Chun He(何鎏春)[1]
Wei-Ping Lin(林炜平)[2] Chuan-Ye Liu(刘传业)[1] Isao Tanihata(谷畑勇夫)[1] Satoru Terashima(寺嶋知)[1]
Yi Tian(田怡)[1] Feng Wang(王枫)[1] Meng Wang(王萌)[1] Guang-Xin Zhang(张广鑫)[1]
Xue-Heng Zhang(章学恒)[2] Li-Hua Zhu(竺礼华)[1] Li-Min Duan(段利敏)[2] Rong-Jiang Hu(胡荣江)[2]
Zhong Liu(刘忠)[2] Chen-Gui Lu(鲁辰桂)[2] Pei-Pei Ren(任培培)[2] Li-Na Sheng(盛丽娜)[2]
Zhi-Yu Sun(孙志宇)[2] Shi-Tao Wang(王世陶)[2] Tao-Feng Wang(王涛峰)[1]
Zhi-Guo Xu(徐治国)[2] Yong Zheng(郑勇)[2]

[1] School of Physics and Nuclear Energy Engineering, Beihang University, Beijing 100191, China
[2] Institute of Modern Physics, Chinese Academy of Sciences, Lanzhou 730000, China

Abstract: Plastic scintillation detectors for Time-of-Flight (TOF) measurements are almost essential for event-by-event identification of relativistic rare isotopes. In this work, a pair of plastic scintillation detectors of dimensions 50 × 50 × 3^t mm^3 and 80 × 100 × 3^t mm^3 have been set up at the External Target Facility (ETF), Institute of Modern Physics (IMP). Their time, energy and position responses are measured with the ^{18}O primary beam at 400 MeV/nucleon. After off-line corrections for walk effect and position, the time resolutions of the two detectors are determined to be 27 ps (σ) and 36 ps (σ), respectively. Both detectors have nearly the same energy resolution of 3.1% (σ) and position resolution of about 3.4 mm (σ). The detectors have been used successfully in nuclear reaction cross section measurements, and will be be employed for upgrading the RIBLL2 beam line at IMP as well as for the high energy branch at HIAF.

Keywords: plastic scintillator, Time-of-Flight, time resolution, walk effect correction

PACS: 29.27.Ac, 29.40.Mc, 29.85.+c **DOI:** 10.1088/1674-1137/41/6/066001

1 Introduction

Plastic scintillation detectors with fast timing are almost essential for Time-of-Flight (TOF) determinations of charged particles at relativistic energies of a few hundred MeV/nucleon, aiming for unambiguous particle identification [1, 2]. Taking nuclear fragmentation as an example, the initial velocities of the reaction products in this process are the same as the velocities of the incident ions. This means that at a few meters' distance the TOF differences between reaction products is only of the order of a few ns.

To improve the TOF resolution, a long flight path length of several tens of meters is generally needed to separate different ions. An alternative way to enhance the TOF resolution is clearly to improve the precision in time determination of TOF. This sometimes gets more important due to the limited flight path. The improved TOF resolution also opens many new opportunities, one of which is the direct mass measurement of exotic nuclei [3–10].

The recent development of plastic scintillators with fast decay times and high-speed photomultiplier tubes (PMT) gives us the opportunity to perform fast timing measurements with a resolution down to about 10 ps (σ). To achieve such a goal, the size of the plastic scintillator has to be minimized, because the time resolution significantly degrades when the scintillator length is increased. For instance, 15 × 25.4 × 0.254^t mm^3 [5], 30 × 20 × 0.5^t mm^3 [11], and 30 × 10 × 3^t mm^3 [12] have been used to reach 10 ps resolution, respectively. In reality, such size detectors are installed at the focal planes of fragment separators where the beam is focused and centered well to a small size.

In current radioactive beam experiments, the secondary heavy ions typically have a relatively large spread

---

Received 28 September 2016, Revised 19 January 2017

∗ Supported by National Natural Science Foundation of China (11475014,11235002) and National Key Research and Development Program (2016YFA0400500)

1) E-mail: bhsun@buaa.edu.cn(Corresponding author)

in both space and angle. In many reaction studies, however, a parallel beam is preferred. In these cases, a plastic scintillator with size of 50 mm × 50 mm or larger is required to fully cover the beam size of secondary ions for particle counting and identification. The standard technique of using such a size of plastic scintillator read out by two or four photomultiplier tubes can give a typical time resolution of about 100+ ps, which is sufficient to discriminate light relativistic radioactive ion species [13]. However, when going to a heavier system with mass number $A > 100$ of interest, a time resolution of less than 50 ps is required, in particular for short flight paths, such as RIBLL2 at IMP.

As a natural extension to the conventional scheme with two or four high-precision measurements of the same physical event, it is possible to gain better time resolution by increasing the active area covered by PMTs. This approach has been tested recently using a circular (27 cm diameter) BC-420 plastic-scintillator sheet read out by 32 photomultiplier tubes, and a time resolution down to the order to 10 ps (1 σ) has been achieved [14].

For the design of large plastic scintillation detectors, the thickness of the plastic scintillator is one of the critical parameters. Although less material in the beam line is generally desired, to avoid extra interactions and energy straggling of the incident beam, a worse time resolution is expected with a thin scintillator, due to fewer photons being emitted and thus smaller pulse height. Indeed, as the thickness of scintillator increases the time resolution is improved accordingly [14, 15]. Moreover, a combination of time-to-analog converter (TAC) with anolog-to-digital converter (ADC) currently has an advantage over time-to-digital converter (TDC) for signal digitization due to better sampling resolution. Attempts [16, 17] have also been made by replacing the conventional electronics by waveform digitizers, which have clear advantages in recording the full event signals but so far are still limited by their sampling rates.

In this work, we report a new investigation of plastic scintillation detectors with relatively large sizes. They satisfy the requirements for detecting relativistic heavy ions: large spreads in space, angle and energy deposited, and excellent timing for particle identification of heavy ions, while minimizing the number of PMTs and electronics used. This work is complementary to previous investigations [5, 11, 12, 14, 15, 18] in terms of thicknesses and sizes of scintillators, types and energies of primary beams, and total energy losses in plastic scintillators, but uses the same types of plastic scintillators and PMTs. Especially, we present the main procedure and details of how to improve the time resolution using the valuable pulse-height and position information. The detectors have already been successfully employed to study nuclear charge radii [19], in which a large coverage of reaction products is crucial. Similar detectors will be used for upgrading the RIBLL2 beam line at IMP, and be a key component of the future high-energy fragment separator at HIAF.

This paper is organized as follows. The experiment is introduced in Section 2. The results and the data analyses of the TOF resolution, energy resolution and position resolution are presented in detail in Section 3. Finally, a summary is given in Section 4.

2 Experiment

The experiment was performed at the Heavy Ion Research Facility in Lanzhou (HIRFL) [20]. The HIRFL is a major facility of the National Laboratory of Heavy Ion Accelerators in China. It consists of Electron Cyclotron Resonance (ECR) ion sources, Sector Focus Cyclotron (SFC), Separated Sector Cyclotron (SSC) and Cooler Storage Ring (CSR) system. The CSR is a double cooler-storage-ring system consisting of a main ring (CSRm), an experimental ring (CSRe), and a radioactive beam line (RIBLL2) to connect the two rings [21]. In this work, the ^{18}O primary beam at 400 MeV/nucleon was extracted from the the CSRm, and then was separated according to magnetic rigidity by using the RIBLL2.

The layout of the apparatus is shown in Fig. 1. The detectors were mounted at the External Target Facility (ETF) [22]. One plastic scintillator (PL0) with a cross-section of 100 mm × 100 mm and a thickness of 3 mm installed at F1 was used as the TOF start. This start detector was designed based on an EJ-200 plastic scintillator bar. One PMT, type Hamamatsu R7111, was used to give the signals from one end of the scintillator.

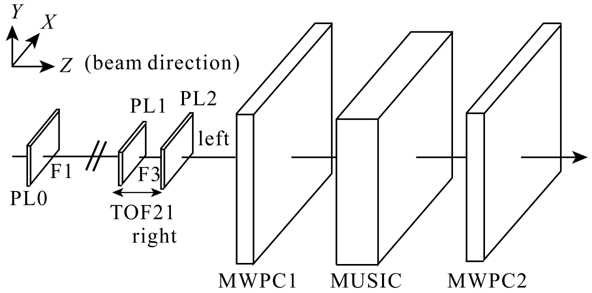

Fig. 1. Schematic view of the experimental setup for the TOF test experiment at RIBLL2. The PMTs are mounted to plastic scintillators in the x-direction.

The plastic scintillation detectors (PL1 and PL2) for testing in the present work were installed at F3, about 26 meters away from PL0 [23]. The sizes of PL1 and PL2 are 50 mm × 50 mm and 80 mm × 100 mm, respectively. Their thickness are fixed to 3 mm. Both ends of PL1 were coupled with PMTs of type H2431 through optical silicone rubber EJ-560. Light guides together with the optical cement EJ-500 were used to match PMT H2431 and the scintillator for PL2 in order to improve the efficiency of light transmission. As for the corresponding plastic scintillators, PL1 is EJ-232Q while PL2 is EJ-232. EJ-232Q (with 0.5% quenching level of benzophenone) is a quenched version of EJ-232. PL1 was also used as the trigger detector for this work. The scintillators were wrapped with aluminum foils, and then with black plastic fabric for light-tightness.

The position information of each ion was determined by two multi-wire proportional chambers (MWPC1 and MWPC2) placed after the plastic scintillation detectors, while in between a multiple sampling ionization chamber (MUSIC) [24] was installed to get the energy deposited by particles of interest. All the position information shown below is deduced from MWPC1 and MWPC2.

Signals from each PMT were split into two, to provide both energy and time information. One was delivered to a Charge-to-Digital Converter (QDC) CAEN v792 for energy loss measurement. The other signal was first fed into a leading edge discriminator (LED) CAEN v895, then again split into two: one to the Time-to-Digital Converter (TDC) CAEN v775 and the other to the Multi-Hit/Multi-Event Time to Digital Converter (Multihit TDC) CAEN v1290. The discriminator thresholds of CAEN v895 were set as low as possible but above the noise level of the PMTs. The full range of the TDCs was set to be 280.4 ns, corresponding to a least significant bit (LSB) of 68.5 ps. Its time calibration was done by using the time calibrator ORTEC-462 and Octal Gate and Delay Generator GG8020 [25]. The Multihit TDC, having a LSB of 25 ps, was used as a cross-check and for pile-up event rejection, and its full scale range was set to 45 μs.

3 Data analysis and results

The energy loss of the ^{18}O beam at 400 MeV/nucleon in both PL1 and PL2 is about 64 MeV. This corresponds to about 1 MeV equivalent electron energy for calculating the relative light output, resulting in a photon yield of about 9000 for PL1 and 3000 for PL2 [13, 26, 27] per incident ^{18}O ion.

The timing is obtained by taking the average from the left- and right-hand PMTs (see Fig. 1). For example, the raw timing for PL1 ($T_{\rm 1raw}$) is eventually calculated as

$$T_{\rm 1raw} = (T_{\rm 1L} + T_{\rm 1R})/2, \tag{1}$$

where $T_{\rm 1L}$ and $T_{\rm 1R}$ are the timing determined from the left-hand and right-hand PMT, respectively.

For each ion hitting the scintillator bars, the integrated charge $Q_{\rm L}$ ($Q_{\rm R}$) obtained from the left (right) side of the plastic scintillators is proportional to the relational expression of the total energy loss Q_0 and the hit position x:

$$\begin{aligned} Q_{\rm L} &= A_{\rm L} Q_0 {\rm e}^{-\lambda x}, \\ Q_{\rm R} &= A_{\rm R} Q_0 {\rm e}^{-\lambda (L-x)}. \end{aligned} \tag{2}$$

Here λ represents the light attenuation parameter, which depends on the scintillator bar. L is the full length of the plastic scintillation bar. $A_{\rm L}$ ($A_{\rm R}$) is the gain coefficient. The deposited energy information in the plastic scintillator is then evaluated as the geometrical mean value $\bar{Q}$:

$$\bar{Q} = \sqrt{Q_{\rm L} \cdot Q_{\rm R}}. \tag{3}$$

The pedestals for QDC need to be subtracted when calculating the integrated charge.

3.1 Time resolution

3.1.1 Walk effect and position correction

For precise determination of the intrinsic time resolution of plastic scintillation detectors, one needs careful investigation of time walk effect due to the variation of pulse amplitudes, and of the effect due to different hitting positions on the plastic scintillators. Both effects can have significant influence on the time resolution. Previous investigations found that simultaneous measurements of both time and pulse-height are very valuable for correction of the walk effect [11, 12].

Taking PL2 as an example, the time dependence on the pulse height can be clearly seen in Fig. 2(a). To correct this walk effect, we use the following formula, proposed in Ref. [12]:

$$T_{\rm walk} = T_{\rm raw} - \frac{C_{\rm raw}}{\sqrt[4]{Q_{\rm L} \cdot Q_{\rm R}}}, \tag{4}$$

where $T_{\rm raw}$ and $T_{\rm walk}$ are the measured timing and the corrected timing with pulse-height, respectively. $C_{\rm raw}$ is the walk effect correction coefficient. It was determined by using only those events hitting a fixed x-position of plastic scintillator. The plot after walk effect correction is shown in Fig. 2(b). Clearly, a large portion of pulse-height dependence can be removed.

However, as shown in Fig. 3, a distinct x-position dependence is still seen after walk effect correction. Considering the fact that ions hitting different positions will result in a different travel time towards both PMTs, the following equation has been applied to eliminate such an effect [28]:

$$T_{\rm corr} = T_{\rm walk} - a \cdot x, \tag{5}$$

where $T_{\rm corr}$ is the time after position correction and a is the correction parameter to be determined from the experimental data. A further check of the data shows there is no dependence of timing on the y-axis of hit position. This is easy to understand considering that the y-dependence will be washed out during the multiple reflections of the light transmitted from the hit position to the PMTs.

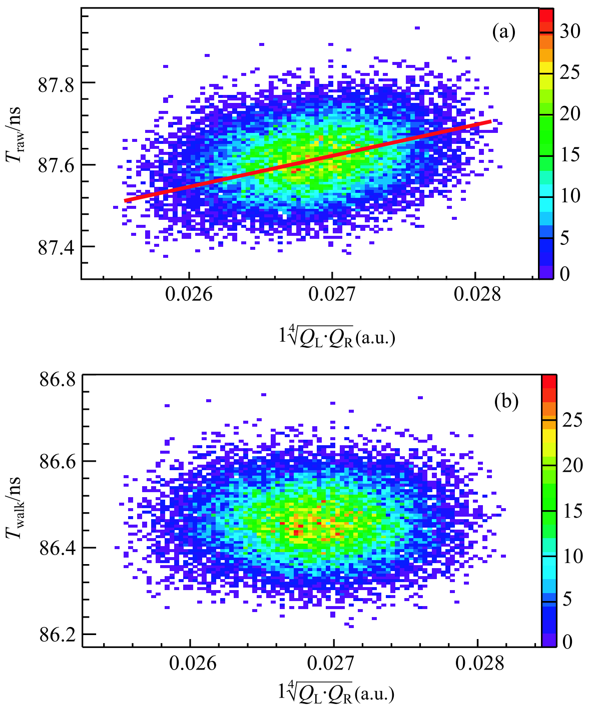

Fig. 2. (color online) Pulse-height dependence of the timing before (a) and after (b) walk effect correction. The red line indicates the linear fit.

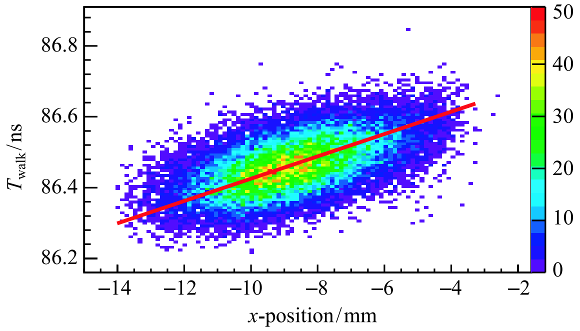

Fig. 3. (color online) Position dependence of the timing after walk effect correction. The red line indicates the linear fit.

With both walk effect and position correction, the timing shows no dependence on either the variation of pulse amplitude or the hit positions. From this we can extract the intrinsic time resolution of the detector, including the contributions of the plastic scintillator, PMT and electronics.

3.1.2 TOF measurements

The TOF distribution can be described very well by a Gaussian function. Taking TOF21, defined as T_2-T_1, as an example, Fig. 4 shows the TOF21 distributions in cases without correction, with only walk effect correction and with both walk effect and position correction. The Gaussian fits (dashed lines) for the three cases show a standard deviation (σ) of 51 ps, 46 ps and 45 ps, respectively.

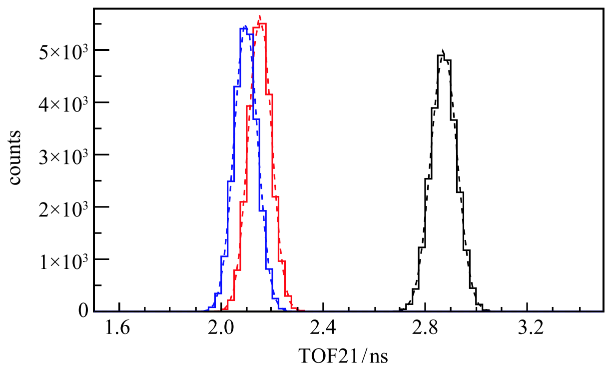

Fig. 4. (color online) TOF21 distributions without correction (black line), with only walk effect correction (blue line) and with both walk effect and position correction (red line). The Gaussian fits (dashed lines) for the three cases are shown.

The resolutions of TOF21, TOF10 and TOF20 are obtained as 45 ps (σ), 83 ps (σ) and 87 ps (σ), respectively. The time resolution of PL1 and PL2 can be calculated by the following formula:

$$\begin{aligned}\sigma_{12}^2&=\sigma_1^2+\sigma_2^2,\\ \sigma_{10}^2&=\sigma_1^2+\sigma_0^2,\\ \sigma_{20}^2&=\sigma_2^2+\sigma_0^2,\end{aligned}\qquad(6)$$

where σ_{12}, σ_{10} and σ_{20} stand for the Gaussian fitting standard deviation (σ) of TOF21, TOF10 and TOF20. σ_1, σ_2 and σ_0 represent the time resolution of PL1, PL2 and PL0, respectively. The resolutions determined for these three detectors are 27 ps (σ), 36 ps (σ) and 79 ps (σ), respectively.

To verify this result, the data registered by Multihit TDC are analyzed as well. 50 ps resolution (σ) for the TOF21 is obtained by using the Multihit TDC data. This is fully consistent with that from the TDC.

3.2 Energy resolution

The energy loss of each ion in the detector can be described by Eq. (3). Shown in Fig. 5 is the energy resolution of PL1.

Both PL1 and PL2 have nearly the same energy resolution of 3.1% (σ) for the ^{18}O primary beam at 400 MeV/nucleon. Such a fast plastic scintillator can be useful for both timing and energy determination identification for light ions.

3.3 Position resolution

The precise hit position on the x-axis of each incident ion on the plastic scintillation detectors is extrapolated from the pair of MWPCs placed right behind. In this work, the intrinsic position resolutions of the MWPCs are determined to be better than 0.9 mm (σ). This resolution is necessary to accurately measure the position resolution of PL1 and PL2.

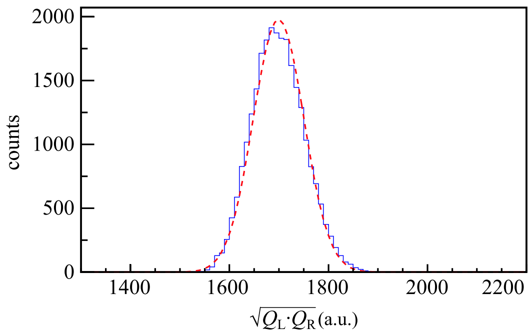

Fig. 5. (color online) The energy resolution of PL1 is about 3.1% (σ), deduced by Gaussian fit.

Taking PL1 as an example here, to investigate the position resolution, six "point" sources, sampled at an intervals of 2 mm along the detector, have been simulated by restricting the incident ions to a well defined region (1 mm width along the x-axis). A similar approach was used in e.g. Ref. [29].

The incident position x on the scintillator bar is usually determined from the timing difference between $T_{\rm L}$ and $T_{\rm R}$,

$$x=b_0+v\cdot\frac{(T_{\rm L}-T_{\rm R})}{2}=b_0+v\cdot\frac{\Delta T}{2}, \tag{7}$$

where b_0 is the offset and v is the effective speed of the signal propagation along the scintillator bar.

While using the leading edge discriminator, the time walk effect caused by the variation of pulse amplitudes would lead to an overestimated position resolution. Thus for precise determinations of ΔT, this effect should be corrected. This amplitude correction can be carried out by fitting the scatter plot of the time versus amplitude of each PMT at a fixed position with the following equation:

$$T=d_0+\frac{d_1}{\sqrt{Q}}. \tag{8}$$

Here Q is the amplitude of the signal and d_0, d_1 are the parameters to be determined.

The distribution of $(\Delta T/2)$ after amplitude correction is shown in Fig. 6(a). Here the incident positions are limited to the range −10.5 mm to −9.5 mm. The mean value and the standard deviation of the distribution, determined from a Gaussian fit, represent the centroid hitting position and its corresponding position resolution, respectively. The average value of the standard deviation of $(\Delta T/2)$ from all six "points" is $\sigma_{\Delta T/2}=34$ ps. Plotted in Fig. 6(b) is the $(\Delta T/2)$ as a function of hit position on the detector. The x-position uncertainty is calculated as the root mean square value of ion distribution in each "point", and it amounts to about 0.3 mm. The speed v of the signal propagation along the detector, 141 mm/ns, is determined from the linear fit. Thus the position resolution (σ) along the detector (x) can be estimated as $\sigma_x=v\cdot\sigma_{\Delta T/2}=4.8$ mm for PL1. A position resolution of 5.1 mm (σ) is obtained for PL2 following the same procedure as PL1. This position resolution estimation also includes the contributions from the uncertainty of hit position resolution determined by the MWPCs and their angular distributions. Therefore the intrinsic resolution should be better than 4.8 mm (σ) for PL1 and 5.1 mm (σ) for PL2.

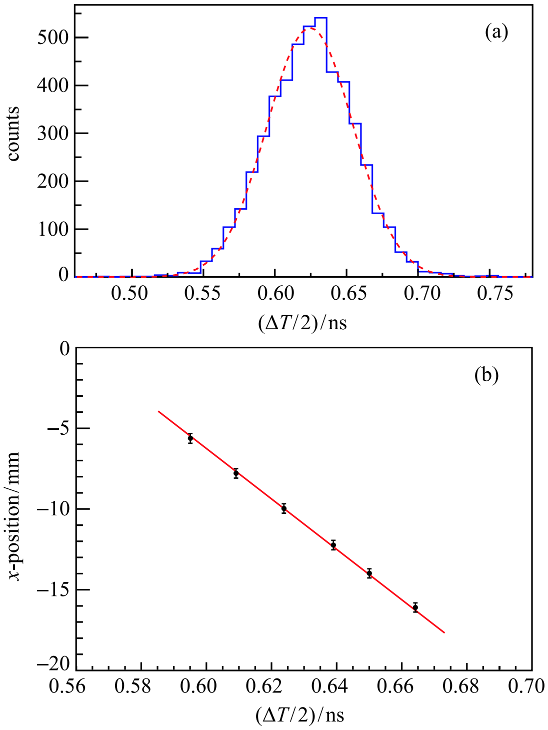

Fig. 6. (color online) (a) $(\Delta T/2)$ distribution (solid line) after amplitude correction with x ranging from −10.5 mm to −9.5 mm. The Gaussian fit to the data is indicated as the dashed line. (b) Plot of x-position vs. $(\Delta T/2)$. The linear fit is also shown.

An alternative way to evaluate the position is to use the integrated charge information from the left-hand and right-hand PMTs, $Q_{\rm L}$ and $Q_{\rm R}$. Following Eq. (2), the horizontal hit position x can be obtained by

$$x\propto\ln(Q_{\rm L}/Q_{\rm R}). \tag{9}$$

Using the same procedure as $(T_{\rm L}-T_{\rm R})$, the $\ln(Q_{\rm L}/Q_{\rm R})$ distribution of PL1 with incident positions in the range −10.5 mm to −9.5 mm is shown in Fig. 7(a). The average standard deviation of $\ln(Q_{\rm L}/Q_{\rm R})$, determined from a Gaussian fit for all six "points", is 0.068. Plotted in Fig. 7(b) is $\ln(Q_{\rm L}/Q_{\rm R})$ as a function of hit position on PL1. The linear coefficient is determined to be 46.7 mm, resulting in a position resolution of 3.2 mm (σ) for PL1. For PL2 the position resolution is calculated as 3.4 mm

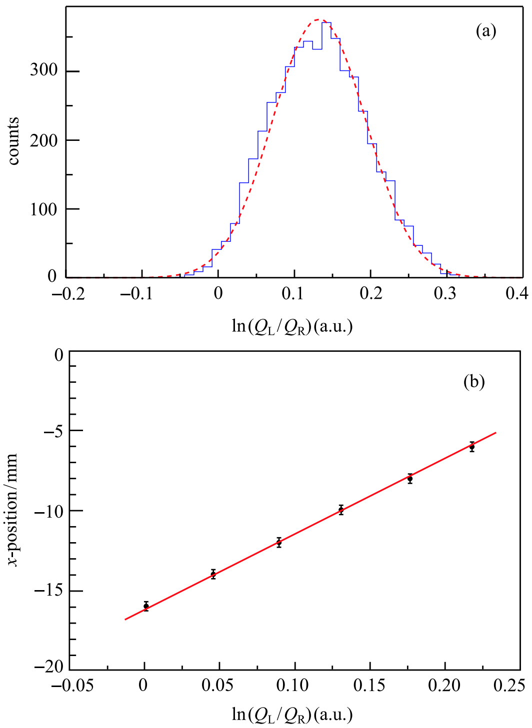

Fig. 7. (color online) (a) $\ln(Q_{\rm L}/Q_{\rm R})$ distribution (solid line) with x ranging from–10.5 mm to–9.5 mm. The Gaussian fit to the data is indicated as the dashed line. (b) Plot of x-position vs. $\ln(Q_{\rm L}/Q_{\rm R})$. The linear fit is also shown.

(σ). These resolutions are significantly better than those obtained from ($T_{\rm L}-T_{\rm R}$), indicating that the ratio of integrated charge from both PMTs is more sensitive to the incident position for detectors of the present size (50 mm × 50 mm and 80 mm × 100 mm).

4 Summary

To summarize, a pair of plastic scintillation detectors with dimensions of 50 × 50 × 3^t mm^3 and 80 × 100 × 3^t mm^3 were tested with a ^{18}O primary beam at 400 MeV/nucleon. Time resolutions of 27 ps (σ) and 36 ps (σ) were obtained after walk effect and position corrections for these two detectors. The results for the time resolution were verified by using the Multihit TDC as a cross check. Both detectors have the same energy resolution of 3.1% (σ). A position resolution of 3.2 mm (σ) for PL1 and 3.4 mm (σ) for PL2 were obtained using the ratio of integrated charge from both PMTs. These resolutions have also been demonstrated in two secondary beam experiments at 200–400 MeV/nucleon. This makes fast plastic scintillators possible for simultaneous measurement of energy deposited, and accordingly, with reasonable precision, the charge and position of incident ions. Such detectors will be used for upgrading the RIBLL2 beam line at IMP and are one of the key components for the high-energy fragment separator at HIAF.

The authors would like to thank the RIBLL collaboration and the HIRFL-CSR team for providing a stable beam and assistance during the experiments.

References

1 B. Voss et al, Nucl. Instrum. Methods A, **364**: 150–158 (1995)
2 J. Kurcewicz et al, Phys. Lett. B, **717**: 371–375 (2012)
3 D. Lunney, J. M. Pearson, and C. Thibaut, Review of Modern Physics, **75**: 1021–1082 (2003)
4 Z. Meisel and S. George, International Journal of Mass Spectrometry, **394**: 145–150 (2013)
5 M. Matos et al, Nucl. Instrum. Methods A, **696**: 171–179 (2012)
6 B. H. Sun et al, Front. Phys., **10**: 1–25 (2015)
7 B. H. Sun et al, EPJ Web Conf., **109**: 04008 (2016)
8 B. Sun et al, Nuclear Physics A, **812**: 1–12 (2008)
9 B. Sun et al, Int. J. Mod. Phys. E, **18**: 346–351 (2009)
10 B. Sun et al, Chin. Phys. C, **33**: 161–163 (2009)
11 S. Nishimura et al, Nucl. Instrum. Methods A, **510**: 377–388 (2003)
12 J. W. Zhao et al, Nucl. Instrum. Methods A, **823**: 41–46 (2016)
13 W.R. Leo, *Techniques for Nuclear and Particle Physics Experiments* (Second edition, Berlin: Springer Verlag, 1994), p.157–175
14 A. Ebran et al, Nucl. Instrum. Methods A, **728**: 40–46 (2013)
15 S. Nakajima et al, Nucl. Instrum. Methods B, **266**: 4621–4624 (2008)
16 S. L. Li et al, Chin. Phys. C, **37**: 016003 (2013)
17 J. J. Wu et al, Chin. Phys. C, **32**: 186–190 (2008)
18 R. Hoischen et al, Nucl. Instrum. Methods A, **654**: 354–360 (2011)
19 B. H. Sun et al, Phys. ReV. C, **90**: 054318 (2014)
20 J. W. Xia et al, Nucl. Instrum. Methods A, **488**: 11–25 (2002)
21 Y. J. Yuan et al, Nucl. Instrum. Methods B, **317**: 214–217 (2013)
22 Z. Y. Sun et al, Phys. Rev. C, **90**: 4 (2014)
23 X. H. Zhang et al, Chin. Phys. C, **37**: 056002 (2013)
24 X. H. Zhang et al, Nucl. Instrum. Methods A, **795**: 389–394 (2015)
25 http://www.ortec-online.com/Products-Solutions/view-model.aspx
26 R. Madey et al, Nuclear Instruments and Methods, **151**: 445–450 (1978)
27 K. Nakayama, E.F. Pessoa, and R. A. Douglas, Nuclear Instruments and Methods, **190**: 555–563 (1981)
28 C. Wu et al, Nucl. Instrum. Methods A, **555**: 142–147 (2005)
29 D. Denisov et al, Nucl. Instrum. Methods A, **823**: 120–125 (2016)